Searching for Ursa Minor Stars at Large Radii

Xuanqi Wei,[1] Nathan R. Sandford,[1] and Ting S. Li[1]

[1] *David A. Dunlap Department of Astronomy and Astrophysics, University of Toronto, 50 St. George Street, Toronto ON, M5S 3H4, Canada*

ABSTRACT

The study focuses on the characterization of stellar membership in the Ursa Minor Dwarf Galaxy (UMi), with a particular emphasis on identifying potential members located in the galaxy's outskirts. Using data obtained from a Dark Energy Spectroscopic Instrument (DESI) Tertiary Program, which includes 6548 stars, we applied a Gaussian mixture model combined with Markov Chain Monte Carlo sampling to estimate the membership probabilities based on radial velocities and metallicities from DESI, and proper motions from GAIA. Stars with a membership probability threshold greater than 0.7 were further analyzed, leading to the confirmation of 2851 members within 18 half-light radii (r_h). To explore the outskirts, we used DESI Jura dataset and extended our search to stars beyond 20 r_h. Through this analysis, four potential outskirt members were identified, whose kinematics and chemodynamics align with those expected of UMi members.

Keywords: Dwarf galaxies, Local Group, Stellar Populations

1. INTRODUCTION

One of the central challenges in studying dwarf galaxies is determining the membership and spatial distribution of their stars, especially in the outskirts, where the gravitational pull of the galaxy weakens, and external forces such as mergers, ram pressure stripping, tidal interaction, and re-ionization become more pronounced (Grebel et al. 2003; Kazantzidis et al. 2010; Fattahi et al. 2018; Wheeler et al. 2019). These processes can significantly shape the morphology and stellar distribution within these galaxies, often manifesting most prominently in their outskirts (Higgs et al. 2021).

Recent advancements in astrometric and photometric data, particularly from the Gaia mission, have enabled the detection of stars in the extreme peripheries of dwarf galaxies. For instance, Chiti et al. (2021) identified member stars up to nine half-light radii from the center of the Tucana II dwarf galaxy, suggesting that such stars might result from merger events or feedback-driven processes. Similarly, Filion & Wyse (2021) and Longeard et al. (2022) analyzed the chemo-dynamical properties of Boötes I, proposing that the system might have been more massive in the past and that tidal stripping has affected the satellite. Yang et al. (2022) explored the red giant branch of Fornax and identified a break in the density distribution, which they interpreted as an extended stellar halo up to a distance of seven half-light radii. Further, Longeard et al. (2023) found new members in Hercules up to ten half-light radii, noting that the lack of a strong velocity gradient argued against ongoing tidal disruption.

The Ursa Minor Dwarf Galaxy (UMi), discovered in 1954, is a spheroidal dwarf galaxy that orbits the Milky Way as one of its satellite galaxies. Due to its proximity, UMi provides an exceptional opportunity to study the dynamics and evolution of dwarf galaxies, which are key to understanding the processes that govern galaxy formation in the universe (McConnachie 2012). UMi is located at a heliocentric distance of approximately 76 ± 10 kpc (McConnachie 2012), making it one of the closer dwarf galaxies available for detailed study. The galaxy exhibits a significant ellipticity of 0.55 ± 0.01, indicating a somewhat elongated shape (McConnachie & Venn 2020a). UMi's mean metallicity of [Fe/H] $= -2.13 \pm 0.01$ reflects its old and metal-poor stellar population (McConnachie & Venn 2020a). The galaxy's dynamical mass within its half-light radius is estimated to be 9.5×10^6 $M_\odot$ (McConnachie 2012), underscoring its dark matter dominance, which is typical of dwarf spheroidal galaxies. Additionally, UMi's proper motion, as measured by Gaia EDR3, provides crucial information about its orbit and interaction history with the Milky Way (Qi et al. 2022). These properties make UMi an excellent candidate for exploring the effects of tidal interactions on its stellar population, particularly in its outermost regions (Figure 1 shows the galactic parameters of Ursa Minor).

In this study, we investigate the structural and kinematic properties of the outer regions of the Ursa Minor Dwarf Galaxy (UMi). The primary goal of this research is to characterize stellar membership in the Ursa Minor

Corresponding author: Xuanqi Wei
henry.wei@mail.utoronto.ca

Dwarf Galaxy, with a particular focus on identifying potential members located in the galaxy's outskirts. We employed data from the DESI Tertiary Program, which includes a dataset of 6548 stars within 18 half-light radii (r_h), to estimate the membership probabilities utilizing a Gaussian mixture model combined with Markov Chain Monte Carlo (MCMC) sampling. To explore the more remote regions of UMi, we utilized the DESI Jura dataset, extending our search to stars located beyond 20 r_h.

Figure 1. The Galactic parameters of Ursa Minor (UMi) include the coordinates α, δ, the mean metallicity, the mean radial velocity (RV), the velocity dispersion, the heliocentric distance $D_\odot$, the ellipticity, the position angle ϕ, and the half-light radius r_h in arcminutes and parsecs (Sestito et al. 2023). Additionally, the mean proper motion from Gaia EDR3, the dynamical mass, the mass density, and the luminosity are reported with their respective references. References are as follows: (a) refers to (McConnachie 2012), (b) to (McConnachie & Venn 2020a), (c) to (McConnachie & Venn 2020b), (d) to (Qi et al. 2022), and (e) to (Mateo 1998).

Property	Value	Reference
α	227.2854 deg	(b)
δ	67.2225 deg	(b)
$\overline{\text{[Fe/H]}}$	-2.13 ± 0.01	(b)
$\overline{\text{RV}}$	246.9 ± 0.1 km s^{-1}	(b)
σ_{V}	9.5 ± 1.2 km s^{-1}	(b)
$D_\odot$	76 ± 10 kpc	(a)
Ellipticity	0.55 ± 0.01	(b)
ϕ	50 ± 1 deg	(b)
r_{h}	17.32 ± 0.11 arcmin	(b)
r_{h}	382 ± 53 pc	(b)
$r_{\text{h, plummer}}$	407 pc	(d)
$\mu_\alpha \cos\delta$	-0.124 ± 0.004 mas yr^{-1}	(c)
μ_δ	0.078 ± 0.004 mas yr^{-1}	(c)
M_{dyn} ($\leq r_{\text{half}}$)	9.5×10^6 M$_\odot$	(a)
Mass density	0.35 M$_\odot$ pc^{-3}	(e)
L	0.29×10^6 L$_\odot$	(e)

This report is structured as follows. In Section 2, we present the data used in this research, following by section 3, the methodology used to complete this research, such as Gaussian Mixture Model, and the 2σ boundary cut. In Section 4, we present the mixture modeling results and potential outskirt members of UMi. In Section 5, we discuss whether the tidal stripping can be found from the potential outskirt members, followed by our conclusion in Section 6.

2. DATA

The Dark Energy Spectroscopic Instrument (DESI) is a state-of-the-art, 5020-fiber spectrograph mounted on the 4-meter Mayall telescope at Kitt Peak National Observatory (Collaboration et al. 2023). DESI's primary mission is to measure the expansion history of the universe with unprecedented precision, but it also plays a crucial role in Galactic astronomy through its Milky Way Survey (DESI-MWS). This survey targets over 7 million stars, focusing on the thick disc and stellar halo of the Milky Way, as well as nearby dwarf galaxies, providing high-quality spectroscopic data (Koposov et al. 2024). The data used in this study comes from DESI's Tertiary Program and DESI Jura dataset, which includes radial velocities, metallicities, and stellar parameters for hundreds of thousands of stars, enabling detailed chemo-dynamical studies of systems like the Ursa Minor Dwarf Galaxy.

2.1. *DESI Tertiary Program for UMi*

The DESI Tertiary Program leverages opportunities when the DESI is not fully operational, such as when only a subset of the instrument's petals are active. This approach ensures that valuable observational time is not wasted, allowing for the continued collection of high-quality spectroscopic data. The program specifically targets objects like the Ursa Minor Dwarf Galaxy during these periods, enabling detailed studies of its stellar population even when DESI's full capacity is not available.

2.2. *DESI Jura*

The DESI Jura dataset is a comprehensive collection that includes Survey Validation (SV) data as well as the entirety of the main and tertiary data gathered between May 14$^{\text{th}}$, 2023, and April 9$^{\text{th}}$, 2024. This dataset is processed using the RVS pipeline, which ensures precise radial velocity measurements (Koposov et al. 2024). It also plays a crucial role in enabling detailed analyses of stellar populations, offering insights into the dynamics and chemical compositions of systems like the Ursa Minor Dwarf Galaxy.

Since the Jura dataset is extremely large, we perform a 10-degree cut from the center of the Ursa Minor Dwarf Galaxy (UMi) to focus our analysis on a more manageable subset of the data. This work has made use of the Local Volume Database[1]. The region of interest is defined by the following constraints on the coordinates:

$$-30^\circ < \alpha_{\text{center}} < 30^\circ \text{ and } -15^\circ < \delta_{\text{center}} < 15^\circ$$

where α represents right ascension (RA) and δ represents declination (DEC). Figure 2 shows the spatial distribution of stars after applying the coordinate transformation, highlighting the selected region within these constraints.

We also account for solar motion by converting the heliocentric radial velocity measurements to the Galactic Standard of Rest (v_{GSR}) frame. This conversion is

[1] https://github.com/apace7/local_volume_database

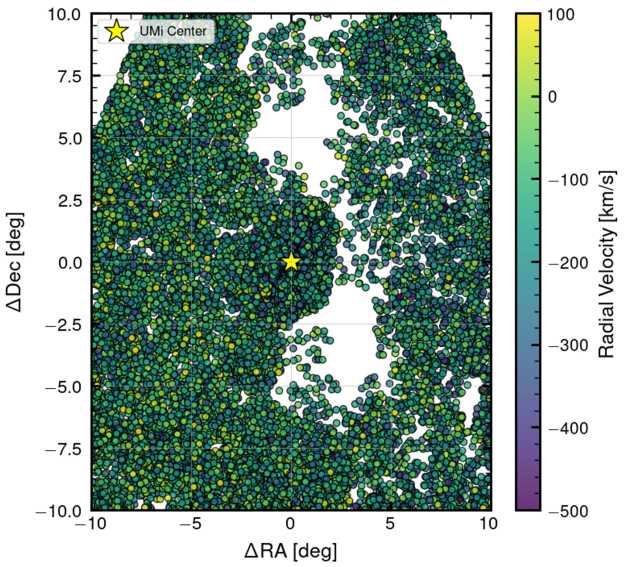

Figure 2. Spatial distribution of stars after coordinate transformation, focusing on the region defined by the constraints. The color of the points indicates the Radial Velocity measured in [km/s]

performed using a function available in the Astropy documentation[2].

2.3. *Data Reduction*

To ensure the quality and reliability of the data, we applied a series of stringent cuts to both the DESI Tertiary and DESI Jura datasets. Specifically, we implemented the following selection criteria:

- VRAD > -600 km s^{-1}
- VRAD < 600 km s^{-1}
- VRAD_ERR < 15 km s^{-1}
- FEH > -3.98
- LOGG < 4
- RVS_WARN $= 0$
- PRIMARY = True (only for DESI Jura)

These cuts ensure that we only include stars with well-measured radial velocities, metallicities, and surface gravities. For the DESI Tertiary dataset, the selection is identical except for the omission of the `PRIMARY = True` criterion. Both datasets follow the radial velocity (RV) pipeline as described in (Koposov et al. 2024), ensuring consistency and accuracy across the data.

[2] Available at https://docs.astropy.org/en/stable/generated/examples/coordinates/rv-to-gsr.html

3. METHODOLOGY

3.1. *Gaussian Mixture Modelling and Markov chain Monte Carlo (MCMC)*

In this study, we apply a combination of Gaussian Mixture Modeling (GMM) and Markov Chain Monte Carlo (MCMC) techniques to characterize the stellar population within the Ursa Minor Dwarf Galaxy (UMi) and estimate the membership probabilities of stars based on their kinematic and chemical properties.

We utilize a Gaussian Mixture Model to describe the distribution of key stellar parameters: heliocentric radial velocity ($v_{\rm hel}$), metallicity ([Fe/H]), and proper motions in right ascension ($\mu_{\alpha*}$) and declination (μ_δ). These parameters are assumed to follow a mixture of two Gaussian distributions, representing the UMi stellar population and the Milky Way field stars.

The radial velocity distribution of UMi stars is modeled using a linear function of the angular distance from the galaxy's center, $v(\phi)$, while the background stars are modeled with a distinct velocity distribution, b_v. For the metallicity distribution, we model it as a function of the ellipticity-corrected radius r_e, parameterized separately for UMi stars and background stars. The proper motions in right ascension and declination are modeled using a bivariate Gaussian distribution that accounts for the correlation between $\mu_{\alpha*}$ and μ_δ. The total likelihood for the GMM is obtained by combining these individual likelihoods.

To explore the parameter space and derive posterior distributions for the model parameters, we implement an MCMC approach. We define prior distributions on the parameters to ensure they remain within physically plausible bounds, with the likelihood function `lnprob` combining the log-likelihoods for radial velocity, metallicity, and proper motions. Parameters that fall outside these prior bounds are penalized, thereby constraining the parameter space. The likelihood function is defined as follows:

$$\ln \mathcal{L}(\theta; v_{\rm hel}, [\mathrm{Fe/H}], \mu_\alpha, \mu_\delta) \quad (1)$$
$$= \ln \left(p_{\rm star} \cdot \mathcal{L}_{\rm star} + (1 - p_{\rm star}) \cdot \mathcal{L}_{\rm back}\right) \quad (2)$$

where the likelihoods $\mathcal{L}_{\rm star}$ and $\mathcal{L}_{\rm back}$ represent the likelihoods given the star belongs to the UMi or the background, respectively. Further details and the derivation of this equation are provided in the Appendix 6.

The MCMC sampling is performed using the `emcee` package (Foreman-Mackey et al. 2013). The initial parameter values are derived from a Nelder-Mead optimization, and the MCMC chains are then evolved over a sufficient number of iterations to ensure convergence to the posterior distribution.

The final posterior distributions from the MCMC analysis are used to compute the membership probability for each star. This is done by evaluating the likelihood of a star belonging to the UMi population relative to the background population. Stars with membership

probabilities exceeding a specified threshold (e.g., 0.7) are classified as members of UMi.

3.2. *Search Members at Outskirt*

To identify potential members of the Ursa Minor Dwarf Galaxy (UMi) in the Jura dataset, a systematic 2σ boundary cut was applied based on the distribution of key stellar parameters such as metallicity ([Fe/H]), radial velocity (RV), and proper motions (PMRA, PMDEC).

Given the mean and standard deviation (σ) values of each parameter — derived from a subset of high-probability UMi members (probability $> 70\%$) from the result of DESI Tertiary Program — the parameters used were as follows:

$$\begin{bmatrix} \text{Mean [Fe/H]} & = -2.22, & \sigma_{\text{[Fe/H]}} = 0.37, \\ \text{Mean RV} & = -243.69\,\text{km/s}, & \sigma_{\text{RV}} = 2.75\,\text{km/s}, \\ \text{Mean PMRA} & = -0.13\,\text{mas/yr}, & \sigma_{\text{PMRA}} = 0.33\,\text{mas/yr}, \\ \text{Mean PMDEC} & = 0.07\,\text{mas/yr}, & \sigma_{\text{PMDEC}} = 0.37\,\text{mas/yr}. \end{bmatrix}$$

For each star in the Jura dataset, we computed the absolute difference between the observed value and the mean for each parameter. Stars were selected if their observed values satisfied the following inequality, which accounts for observational errors (σ_{obs}):

$$|\text{Parameter} - \text{Mean}| < 2 \times \sqrt{\sigma^2 + \sigma_{\text{obs}}^2},$$

where the parameters include [Fe/H], RV, PMRA, and PMDEC, with σ representing the standard deviation obtained from the high-probability UMi stars.

Next, the intersection of the sets of stars that satisfied the above criterion across all parameters was determined to isolate potential UMi members in the Jura dataset.

To further refine this selection, only stars located at distances greater than $20 \times r_{\text{half}}$ (where r_{half} is the half-light radius of UMi) were considered. This selection focuses on stars in the outer regions, where tidal stripping and other external forces are more significant.

The final sample consisted of stars that passed all these criteria, and their relevant spatial and kinematic properties (RA, DEC, [Fe/H], RV, PMRA, PMDEC) were extracted for further analysis.

4. RESULTS

4.1. *Membership Determination*

This section describes the result of the membership confirmation process in identifying and verifying the stars that are most likely associated with the Ursa Minor (UMi) Dwarf Galaxy. To ensure robustness in membership determination, we applied a probability threshold of 0.7, which resulted in the identification of 2,851 stars as probable UMi members following the process describe in 3.1.

We visualized the spatial distribution of the identified members by plotting their positions in relation to the center of the Ursa Minor Dwarf Galaxy. The figure below (Figure 3) demonstrates the concentration of stars with high membership probabilities, with color-coding based on the calculated probabilities. The stars

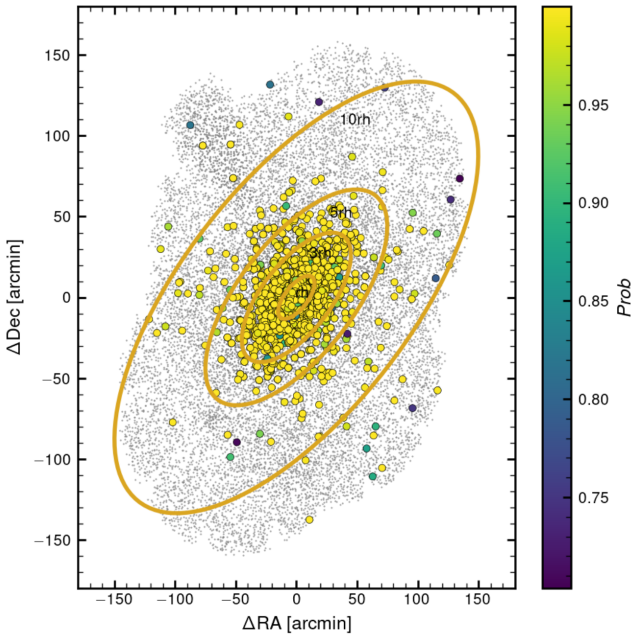

Figure 3. Spatial distribution of probable Ursa Minor Dwarf Galaxy members. The x-axis represents the change in right ascension (ΔRA) and the y-axis the change in declination (ΔDec) from the galaxy center, both in arcminutes. The color of the points indicates the membership probability, with yellow representing the highest probabilities (close to 1) and darker colors representing lower probabilities. The grey scatters represents the whole dataset. The overlaid contours represent the 5 and 10 half-light radii (r_h) of the galaxy, highlighting the concentration of likely members within these regions.

were further analyzed across various parameters including metallicity ([Fe/H]), radial velocity (V_{hel}), proper motion in declination (pmdec), and proper motion in right ascension (pmra) in 4.2.

4.2. *Membership Characterization*

In this section, we're looking at how we've characterized the stars as members of Ursa Minor, using a probability threshold of 0.7. Figure 4 presents scatter plots illustrating various relationships between star parameters in the Ursa Minor Dwarf Galaxy. Each subplot uses a membership probability threshold of 0.7, with the color scale representing the membership probability, ranging from 0.7 to 1.0.

The relationship between metallicity $[Fe/H]$ and elliptical radius (er) in arcminutes is shown as the subplot 1. A slight negative correlation is observed, where stars

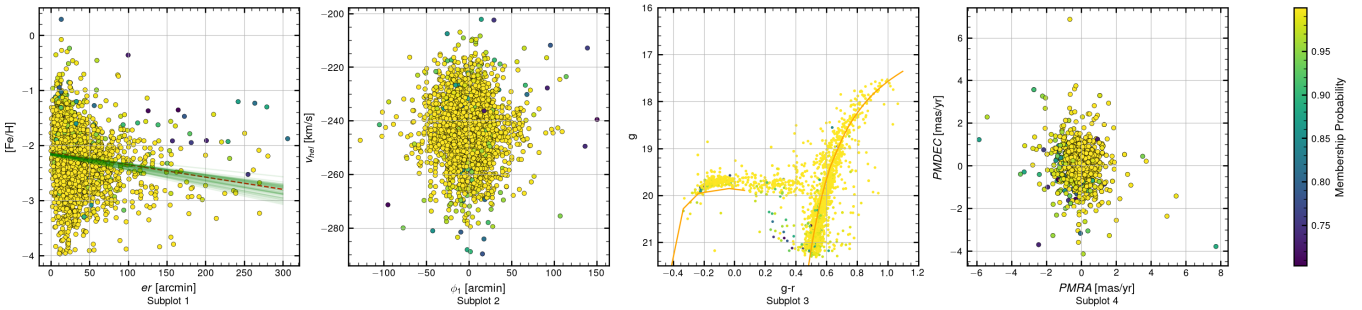

Figure 4. UMi Membership Characterization Scatter Plots. The color scale represents the membership probability, ranging from 0.7 to 1.0. **Subplot 1:** The relationship between metallicity $[Fe/H]$ and elliptical radius (er) in arcminutes. The red dotted line are generated from the Local Volume Database. The green shaded area represents multiple linear fits sampled from the posterior distribution of the model parameters. **Subplot 2:** The heliocentric velocity ($v_{\rm hel}$) against the angular coordinate ϕ_1 in arcminutes. **Subplot 3:** The relationship between the g-band magnitude (g) and the color index (g-r). The overlaid lines represent the isochrones and empirical data from M92. **Subplot 4:** The proper motion in declination (PMDEC) versus proper motion in right ascension (PMRA).

with higher metallicity generally reside at smaller radii, closer to the center of the Ursa Minor Dwarf Galaxy. The green shaded area represents multiple linear fits sampled from the posterior distribution of the model parameters, showcasing the uncertainty in the slope and intercept. This trend suggests that stars closer to the galaxy's core tend to have higher metallicity, consistent with the expectation that the central regions of dwarf galaxies are often more 'metal-rich'.

The calibrated heliocentric velocity ($v_{\rm hel}$) versus the angular coordinate ϕ_1 in arcminutes is shown in subplot 2. The scatter plot reveals no strong correlation between these two parameters. The stars with higher membership probabilities (indicated by yellow points) are evenly distributed across a wide range of ϕ_1 values. This distribution suggests that the stars identified as members of the galaxy do not show a significant velocity gradient across ϕ_1, which might be expected if the galaxy were undergoing coherent rotation or had a significant velocity gradient along this axis.

As for subplot 3, the g-band magnitude (g) versus the color index ($g - r$) is shown. The majority of high-probability members (shown in yellow) align well with the expected stellar locus, tracing a well-defined main sequence. The overlaid lines represent the isochrones and empirical data from M92, which are used to compare the observed stars with theoretical models of stellar evolution. The good agreement between the observed stars and the isochrones reinforces the classification of these stars as members of the Ursa Minor Dwarf Galaxy.

Lastly, subplot 4 presents the proper motion in declination ($PMDEC$) versus proper motion in right ascension ($PMRA$). This plot reveals that most of the stars cluster around low proper motion values, with higher membership probability stars predominantly residing near the center of this distribution. This concentration suggests that proper motion is a crucial factor in determining membership within the Ursa Minor Dwarf Galaxy. The tight clustering indicates that the galaxy's member stars share similar motion through space, distinct from foreground stars or background objects that typically exhibit higher proper motions.

Overall, these plots provide a comprehensive view of the characteristics of stars in the Ursa Minor Dwarf Galaxy, with membership probabilities used to discern likely members from non-members. These characterizations aren't just interesting on their own — they're also crucial for verifying potential Ursa Minor stars in the outskirts, specifically those identified in the Jura dataset. By comparing these patterns, we can more confidently determine if those distant stars are the members of Ursa Minor.

4.3. *Potential Outskirt Members*

In this section, a total of 30 potential UMi stars are identified. The spatial distribution of these potential members (shown in Figure 5), particularly those located beyond 20 elliptical radii, was analyzed using data from the Jura dataset. The selection of these outermost stars was made following the method described in Section 3.2, which ensures that only stars aligning well to the UMi's properties are considered. Specifically, to explore the dynamical behavior of these stars, we generated UMi's orbit using the `galpy` library[3].

The orbit integration was performed by first transforming the systemic velocity of the stars to the Galactic Standard of Rest (GSR) frame. The six-dimensional phase space coordinates of Ursa Minor (including right ascension, declination, distance, proper motions, and systemic velocity) were then used to initialize the orbit object. The orbits were integrated both forward and backward in time over 0.5 Gyr, allowing us to trace the past and future trajectories of these stars. Also, the ellipses overlaid on the figure highlight the structure and extent of the stellar distribution, indicating that these

[3] Available at https://docs.galpy.org/en/v1.7.2/reference/orbit.html

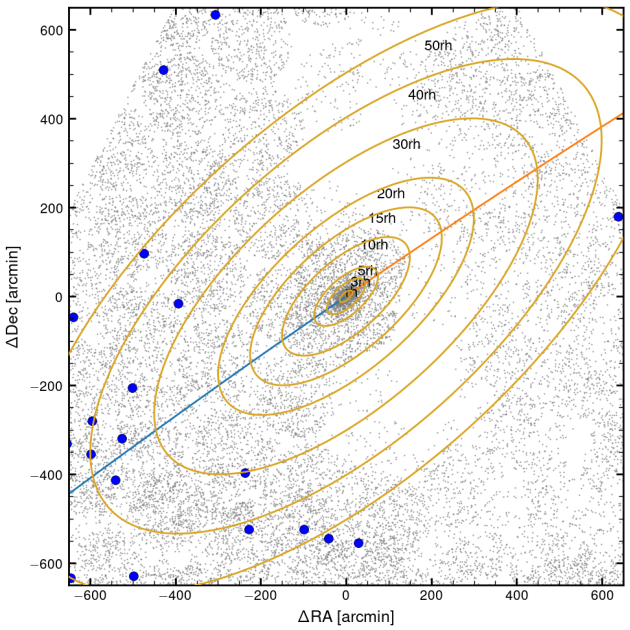

Figure 5. The spatial distribution of potential members of the Ursa Minor Dwarf Galaxy, focusing on stars located beyond 20 elliptical radii. Blue points indicating the potential outskirt member stars' positions. The orange contours represent different radii from the center of the galaxy, labeled at intervals of $3r_h$ to $50r_h$. The blue line and orange represents the orbit.

stars trace an elongated shape that is consistent with the galaxy's orbit.

In the figure 6, a key point to highlight is the process used for the VRAD vs. $\phi 1_{orb}$ plot. In this analysis, we initially compared the observed velocities of potential Ursa Minor members with the predicted velocities along the galaxy's orbit. The red line in the plots represents the predicted line-of-sight velocity (v_{los}) of the orbit, and the dashed lines show a tolerance range of $\pm 2\sigma$, where σ is the standard deviation of the observed velocities (v_{gsr}). However, to improve accuracy, especially for stars located far from the galaxy's center, we later implemented an interpolation method. This interpolation allows us to predict the expected velocity (v_{los}) at the exact position ($\phi 1_{orb}$) of each star, providing a more precise cut criterion for identifying members of Ursa Minor.

The potential outskirt stars, marked in blue, will be further analyzed individually to determine their alignment with the characteristics of UMi stars. This iterative analysis will help confirm whether these outskirt stars are indeed dynamically associated with Ursa Minor. Out of these, we found four stars that stood out as particularly interesting with TargetIDs: 2782289826152448, 2782305093419011, 2782097571840008, and 39089837512662297. These stars align well within the sigma bounds across all the figures, indicating that their properties are consistent

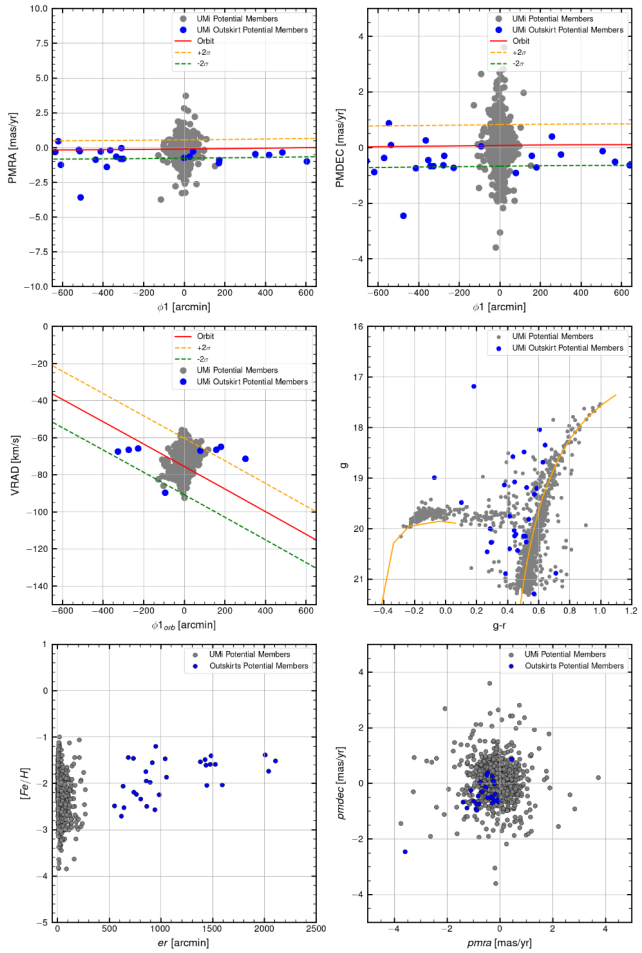

Figure 6. The figure visualizes the properties of 30 potential outskirt members of the Ursa Minor Dwarf Galaxy (UMi), represented by blue points, in comparison to the main population of UMi stars shown as grey points. Each subplot presents different stellar parameters: **Top Left:** Proper motion in right ascension (PMRA) vs. ϕ_1 (arcmin). The solid red line shows the expected orbital trend, while the orange and green dashed lines represent $\pm 2\sigma$ deviations from the orbit. **Top Right:** Proper motion in declination (PMDEC) vs. ϕ_1 (arcmin). The solid red line shows the expected orbital trend, while the orange and green dashed lines represent $\pm 2\sigma$ deviations from the orbit. **Middle Left:** Radial velocity (VRAD) vs. orbital angular coordinate (ϕ_1). The solid red line shows the expected orbital trend, while the orange and green dashed lines represent $\pm 2\sigma$ deviations from the orbit. **Middle Right:** g-band magnitude vs. $g - r$ color index. The orange lines are the isochrones and empirical data from M92. **Bottom Left:** Metallicity ([Fe/H]) vs. elliptical radius (er in arcmin). **Bottom Right:** Proper motion in declination vs. proper motion in right ascension.

with those of Ursa Minor members. Moreover, they also follow the isochrones closely, suggesting that they share the same age and metallicity as other known members.

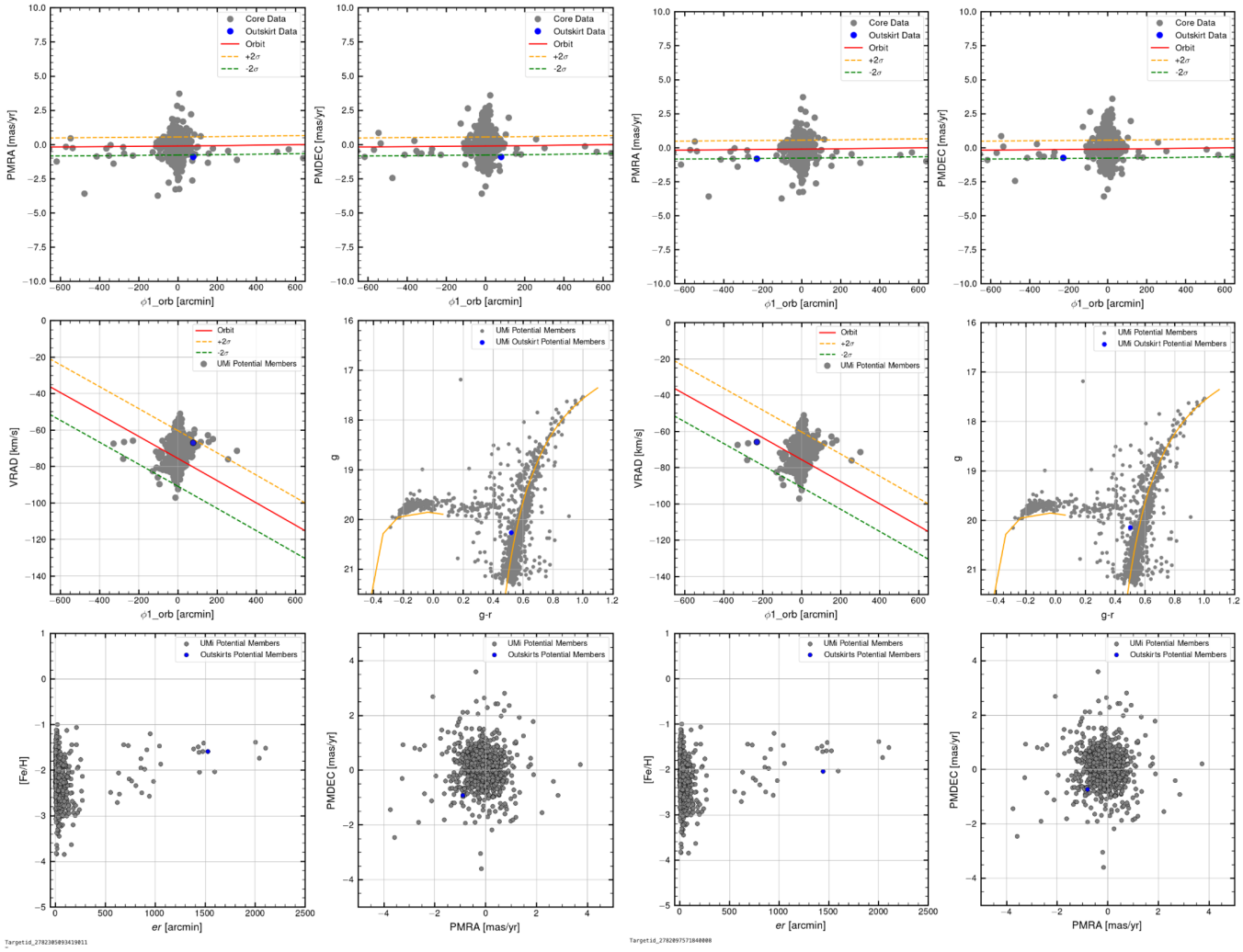

Figure 7. Comparison of two interesting potential outskirt stars (blue points) with the core UMi stars (grey points) across various stellar parameters. TargetIDs 2782305093419011 is shown on the left panel and TargetIDs 2782097571840008 is shown on the right panel. Each row of the figure displays the properties of these stars for the corresponding UMi outskirt candidates same as Figure 6.

The two stars highlighted in the Figure 7 with with the TargetIDs 2782305093419011 and 2782097571840008 show a strong alignment with the characteristic properties of the Ursa Minor Dwarf Galaxy (UMi), suggesting they are likely members of this system despite their location in the galaxy's outskirts. In terms of kinematics, both stars exhibit proper motions in right ascension (PMRA) and declination (PMDEC) that are consistent with the orbital predictions for UMi, falling well within the $\pm 2\sigma$ confidence intervals, as shown in the top row of plots. Additionally, their radial velocities (VRAD) closely follow the expected trend with the orbital angular coordinate (ϕ_1), further reinforcing their potential association with UMi.

Photometrically, the stars' positions in the g-band magnitude versus $g - r$ color index plot closely match the expected stellar locus, as indicated by the orange isochrone. This alignment suggests that these stars have similar stellar populations to those in UMi, which is indicative of their membership.

Finally, the metallicity ([Fe/H]) and elliptical radius (er) of these stars, plotted in the bottom row, also align with the distribution of known UMi stars, particularly for stars situated at larger elliptical radii. Their positions in the PMRA vs. PMDEC plot are consistent with the cluster of UMi stars, further corroborating their likely membership.

Overall, the combination of kinematic, photometric, and chemical properties strongly supports the hypothesis that these two outskirt stars are dynamically associated with the Ursa Minor Dwarf Galaxy.

5. DISCUSSION

5.1. *Tidal Stripping*

The spatial distribution of the four interesting stars identified in this study raises questions about their mem-

bership in the Ursa Minor Dwarf Galaxy (UMi). As shown in Figure 8, these stars are located far from the galaxy's central region, extending beyond 20 half-light radii (r_h). Despite their distance, these stars do not appear to follow the orbital path predicted by tidal stripping models, which suggests that stars should be dispersed along the tidal tails. Their deviation from the expected orbit indicates that these stars might not have been subject to the same tidal forces that affect the majority of UMi's stellar population.

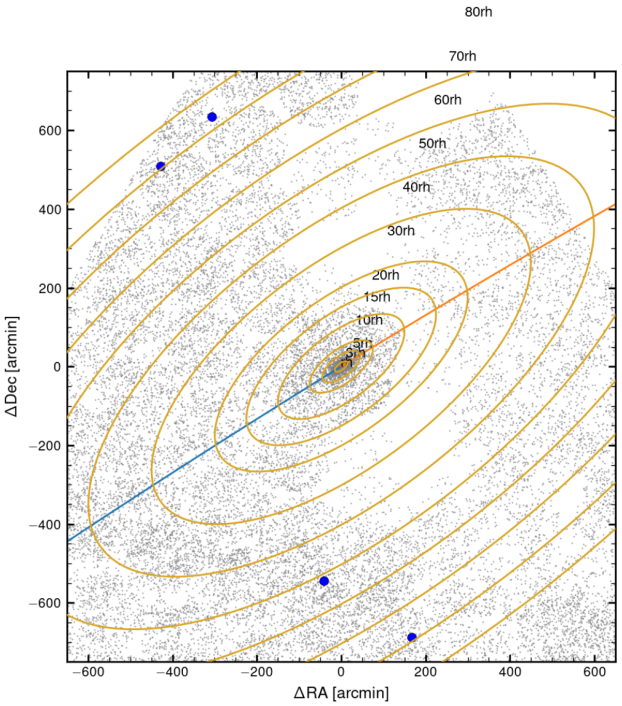

Figure 8. Spatial distribution of four interesting stars (blue points) in relation to the Ursa Minor Dwarf Galaxy (UMi). The figure shows ΔRA versus ΔDec with yellow contours representing different radii from the center of UMi, labeled at intervals of $3r_h$ to $80r_h$. The blue and orange line indicates the expected orbital path of UMi. The highlighted stars are located far from the predicted orbit, suggesting that they do not follow the typical tidal stripping pattern observed in UMi.

Given their position and the lack of alignment with UMi's orbital characteristics, it is possible that these stars are either foreground/background objects or belong to a different stellar population, unassociated with UMi. However, further analysis is required to draw definitive conclusions about their origins and association with the galaxy.

Future work could focus on a detailed tidal analysis to assess whether these stars might still be dynamically connected to UMi through weaker tidal interactions or if they represent an unbound population. To investigate the role of tidal stripping in forming the outskirt members of UMi, a systematic approach can be adopted suggested in (Sestito et al. 2023):

1. Surface Number Density Profile: Derive the surface number density profile and its logarithmic derivative for candidate members of UMi, following the method outlined by (Jensen et al. 2023). This will help identify any departures from an exponential profile, which could indicate the presence of tidal features.

2. Identification of 'Break' Radius: Investigate the existence of a 'break' radius, where the surface density profile flattens, indicating the transition from a bound to an unbound stellar population. The relation from (Peñarrubia et al. 2009) can be used to predict this observational 'break' radius based on the time since UMi's last pericentric passage.

Through these steps, a more comprehensive understanding of the role of tidal interactions in shaping the outer regions of UMi can be achieved. Although tidal stripping is a plausible explanation for the majority of the galaxy's extended halo, the presence of outlier stars, as discussed, suggests that other processes may also be at play.

6. CONCLUSION

In this study, we conducted a detailed analysis of the stellar population in the Ursa Minor Dwarf Galaxy (UMi) to identify potential members, particularly those located in the galaxy's outskirts. By utilizing data from the DESI Tertiary Program and the Jura dataset, we employed a Gaussian Mixture Model combined with Markov Chain Monte Carlo (MCMC) sampling to estimate membership probabilities based on radial velocities, metallicities, and proper motions.

Our analysis confirmed the membership of 2,851 stars within 18 half-light radii (r_h) of UMi, showcasing a comprehensive characterization of these stars' kinematic, photometric, and chemical properties. Additionally, we extended our search to the outskirts of UMi, identifying 30 potential outskirt members, with four stars standing out due to their strong alignment with UMi's expected properties.

However, the spatial distribution and kinematic properties of these four stars suggest that they may not follow the typical tidal stripping patterns expected for UMi members. This raises questions about their true membership and suggests that other processes, such as tidal perturbations or interactions with the Milky Way, could be influencing the outer regions of UMi.

While our current analysis did not include a detailed examination of tidal effects, we propose that future work should focus on this aspect to better understand the mechanisms shaping UMi's extended stellar halo. By analyzing surface number density profiles, identifying potential break radii, and examining logarithmic derivatives, future studies can provide deeper insights into the role of tidal interactions in the evolution of dwarf galaxies like UMi.

Overall, our findings contribute to the ongoing efforts to unravel the complexities of dwarf galaxy evolution, particularly in understanding the dynamics and membership of stars in their outermost regions. The methodologies applied here can be extended to other dwarf galaxies, offering a framework for future studies aimed at exploring the interplay between internal and external forces in shaping these systems.

ACKNOWLEDGMENTS

I would personally like to thank Prof. Ting S. Li, and Dr. Nathan R. Sandford for their invaluable insights and guidance throughout this research. This work was supported by the University of Toronto and the David A. Dunlap Department of Astronomy and Astrophysics. We also acknowledge the use of data from the Dark Energy Spectroscopic Instrument (DESI). Special thanks to Andrew Li who provided his code using Gaussian mixture models and MCMC on Jhelum and Indus as a reference for this study. Additionally, I would like to express my gratitude to Dr. Gustavo E. Medina and Dr. Mairead Heiger for their contributions and support.

Facilities: AAT

Software: astropy (Collaboration et al. 2018), emcee (Foreman-Mackey et al. 2013), matplotlib (Hunter 2007), numpy (Harris et al. 2020), scipy (Virtanen et al. 2020).

REFERENCES

Chiti, A., Frebel, A., Simon, J. D., et al. 2021, Nature Astronomy, 5, 392, doi: 10.1038/s41550-020-01285-w

Collaboration, D., Adame, A. G., Aguilar, J., et al. 2023, The Early Data Release of the Dark Energy Spectroscopic Instrument, doi: 10.5281/zenodo.7964161

Collaboration, T. A., Price-Whelan, A. M., Sipőcz, B. M., et al. 2018, The Astronomical Journal, 156, 123, doi: 10.3847/1538-3881/aabc4f

Fattahi, A., Navarro, J. F., Frenk, C. S., et al. 2018, Monthly Notices of the Royal Astronomical Society, 476, 3816, doi: 10.1093/mnras/sty408

Filion, C., & Wyse, R. F. G. 2021, The Astrophysical Journal, 923, 218, doi: 10.3847/1538-4357/ac2df1

Foreman-Mackey, D., Hogg, D. W., Lang, D., & Goodman, J. 2013, Publications of the Astronomical Society of the Pacific, 125, 306, doi: 10.1086/670067

Grebel, E. K., Iii, J. S. G., & Harbeck, D. 2003, The Astronomical Journal, 125, 1926, doi: 10.1086/368363

Harris, C. R., Millman, K. J., van der Walt, S. J., et al. 2020, Nature, 585, 357, doi: 10.1038/s41586-020-2649-2

Higgs, C. R., McConnachie, A. W., Annau, N., et al. 2021, Monthly Notices of the Royal Astronomical Society, 503, 176, doi: 10.1093/mnras/stab002

Hunter, J. D. 2007, Computing in Science & Engineering, 9, 90, doi: 10.1109/MCSE.2007.55

Jensen, J., Hayes, C. R., Sestito, F., et al. 2023, Small-scale stellar haloes: detecting low surface brightness features in the outskirts of Milky Way dwarf satellites, arXiv, doi: 10.48550/arXiv.2308.07394

Kazantzidis, S., Łokas, E. L., Callegari, S., Mayer, L., & Moustakas, L. A. 2010, The Astrophysical Journal, 726, 98, doi: 10.1088/0004-637X/726/2/98

Koposov, S. E., Allende Prieto, C., Cooper, A. P., et al. 2024, Monthly Notices of the Royal Astronomical Society, 533, 1012, doi: 10.1093/mnras/stae1842

Longeard, N., Jablonka, P., Arentsen, A., et al. 2022, Monthly Notices of the Royal Astronomical Society, 516, 2348, doi: 10.1093/mnras/stac1827

Longeard, N., Jablonka, P., Battaglia, G., et al. 2023, Monthly Notices of the Royal Astronomical Society, 525, 3086, doi: 10.1093/mnras/stad2227

Mateo, M. L. 1998, Annual Review of Astronomy and Astrophysics, 36, 435, doi: 10.1146/annurev.astro.36.1.435

McConnachie, A. W. 2012, The Astronomical Journal, 144, 4, doi: 10.1088/0004-6256/144/1/4

McConnachie, A. W., & Venn, K. A. 2020a, The Astronomical Journal, 160, 124, doi: 10.3847/1538-3881/aba4ab

—. 2020b, Research Notes of the AAS, 4, 229, doi: 10.3847/2515-5172/abd18b

Peñarrubia, J., Navarro, J. F., McConnachie, A. W., & Martin, N. F. 2009, The Astrophysical Journal, 698, 222, doi: 10.1088/0004-637X/698/1/222

Qi, Y., Zivick, P., Pace, A. B., Riley, A. H., & Strigari, L. E. 2022, Monthly Notices of the Royal Astronomical Society, 512, 5601, doi: 10.1093/mnras/stac805

Sestito, F., Zaremba, D., Venn, K. A., et al. 2023, Monthly Notices of the Royal Astronomical Society, 525, 2875, doi: 10.1093/mnras/stad2427

Virtanen, P., Gommers, R., Oliphant, T. E., et al. 2020, Nature Methods, 17, 261, doi: 10.1038/s41592-019-0686-2

Wheeler, C., Hopkins, P. F., Pace, A. B., et al. 2019, Monthly Notices of the Royal Astronomical Society, 490, 4447, doi: 10.1093/mnras/stz2887

Yang, Y., Hammer, F., Jiao, Y., & Pawlowski, M. S. 2022, Monthly Notices of the Royal Astronomical Society, 512, 4171, doi: 10.1093/mnras/stac644

APPENDIX

DETAILED LIKELIHOOD FUNCTION DESCRIPTION

The likelihood function is defined as follows:

$$\ln \mathcal{L}(\theta; v_{\rm hel}, [\mathrm{Fe/H}], \mu_\alpha, \mu_\delta) \tag{1}$$
$$= \ln \left(p_{\rm star} \cdot \mathcal{L}_{\rm star} + (1 - p_{\rm star}) \cdot \mathcal{L}_{\rm back} \right) \tag{2}$$

where the log-likelihood components for the stream and background models are given by:

$$\mathcal{L}_{\rm star} = \ln p_{\rm star} + \ln \mathcal{N}(v_{\rm hel} \mid v_{\rm model}, \sigma_{v_{\rm hel}}) \tag{3}$$
$$+ \ln \mathcal{N}([\mathrm{Fe/H}] \mid [\mathrm{Fe/H}]_{\rm model}, \sigma_{[\mathrm{Fe/H}]}) \tag{4}$$
$$+ \ln \mathcal{N}_2(\mu_\alpha, \mu_\delta \mid \mu_{\alpha,1}, \mu_{\delta,1}, \sigma_{\mu_\alpha}, \sigma_{\mu_\delta}, \rho), \tag{5}$$

$$\mathcal{L}_{\rm background} = \ln(1 - p_{\rm star}) + \ln \mathcal{N}(v_{\rm hel} \mid b_v, \sigma_{v_{\rm hel}}) \tag{6}$$
$$+ \ln \mathcal{N}([\mathrm{Fe/H}] \mid b_{[\mathrm{Fe/H}]}, \sigma_{[\mathrm{Fe/H}]}) \tag{7}$$
$$+ \ln \mathcal{N}_2(\mu_\alpha, \mu_\delta \mid b_{\mu_\alpha}, b_{\mu_\delta}, \sigma_{\mu_\alpha}, \sigma_{\mu_\delta}, \rho). \tag{8}$$

Here, $\mathcal{N}$ and $\mathcal{N}_2$ represent the univariate and bivariate normal distributions, respectively, and ρ denotes the correlation between the proper motion components μ_α and μ_δ. The total likelihood is the combination of the likelihoods for the stream and background models, weighted by the probability $p_{\rm star}$ of belonging to the stream.

In these equations:

- $p_{\rm star}$ is the probability of the star belonging to the stream.
- $v_{\rm hel}$ is the heliocentric velocity.
- [Fe/H] is the metallicity.
- μ_α and μ_δ are the proper motion components in right ascension and declination, respectively.
- $\sigma_{v_{\rm gsr}}$, $\sigma_{[\mathrm{Fe/H}]}$, σ_{μ_α}, and σ_{μ_δ} are the uncertainties in the corresponding measurements.
- $v_{\rm model}$, $[\mathrm{Fe/H}]_{\rm model}$, $\mu_{\alpha,1}$, and $\mu_{\delta,1}$ are the model parameters for the UMi.
- b_v, $b_{[\mathrm{Fe/H}]}$, b_{μ_α}, and b_{μ_δ} are the model parameters for the Milky Way Field Stars.
- ρ is the correlation coefficient between the proper motion components μ_α and μ_δ.